Applied Surface Science 626 (2023) 157136

Contents lists available at ScienceDirect

Applied Surface Science

journal homepage: www.elsevier.com/locate/apsusc

Full Length Article

Tailored wettability in fluorinated carbon nanoparticles synthesized from fluorotelomer alcohols

Enes Muhammet Can [a,b,c,*], Masamichi Nishihara [b,d], Junko Matsuda [b,d], Kazunari Sasaki [b,d,e], Stephen Matthew Lyth [a,b,f,g]

[a] Department of Automotive Science, Graduate School of Integrated Frontier Sciences, Kyushu University, 744 Motooka, Nishi-ku, Fukuoka 819-0395, Japan
[b] Next-Generation Fuel Cell Research Center (NEXT-FC), Kyushu University, 744 Motooka, Nishi-ku, Fukuoka 819-0395, Japan
[c] Mechanical Engineering Department, Faculty of Engineering and Architecture, Kirsehir Ahi Evran University, Kırşehir, Turkiye
[d] International Research Center for Hydrogen Energy, Kyushu University, 744 Motooka, Nishi-ku, Fukuoka 81970395, Japan
[e] Department of Hydrogen Energy Systems, Graduate School of Engineering, Kyushu University, 744 Motooka, Nishi-ku, Fukuoka 819-0395, Japan
[f] Department of Mechanical Engineering, Faculty of Engineering, University of Sheffield, Ella Armitage Building, Sheffield S3 7RD, United Kingdom
[g] Department of Chemical and Process Engineering, University of Strathclyde, Glasgow G1 1XL, United Kingdom

ARTICLE INFO

Keywords:
Carbon nanomaterials
Fluorinated carbon
Superhydrophobicity
Graphitization

ABSTRACT

A simple and unique method is presented for the synthesis of fluorinated carbon nanoparticles via exothermic reaction between fluorotelomer alcohols and sodium metal in a sealed polytetrafluoroethylene crucible. Four different fluorotelomer alcohols are used as precursors to investigate the effect of chain length on the microstructure, chemical structure, and fluorine content of the resulting fluorinated carbons. The materials are confirmed to be highly hydrophobic, and the effect of the selected precursor on water contact angle is elucidated. Interestingly, the fluorinated carbons have highly graphitic regions despite the relatively low reaction temperature, and a new catalytic mechanism for this is proposed. Finally, the effect of secondary heat treatment on the fluorine content and water contact angle is investigated. This work presents an effective method to tailor the fluorine content of carbons via both chemical and thermal methods.

1. Introduction

The incorporation of fluorine atoms can significantly alter the physical, chemical, and electronic properties of carbon-based materials. In particular, fluorination generally leads to enhanced hydrophobicity due to low surface free energy and reduced van der Waals interactions [1]. Fluorinated carbons are attracting considerable attention in applications including tribological coatings [2], electrodes for lithium-ion batteries [3-5], gas sensors [6], polymer electrolyte fuel cells, and water electrolysis [7,8]. A wide range of carbon-based materials have been fluorinated in the literature, with examples including carbon black [9,10], activated carbon [11], carbon fiber [12,13], carbon nanotubes [14,15], and graphene [16,17]. Meanwhile, methods for the fluorination of carbon can be mainly classified into four types: (i) direct fluorination, (ii) indirect fluorination, (iii) plasma fluorination, and (iv) chemical functionalisation. The direct fluorination method involves the direct reaction of fluorine gas (F_2) with the surface of the target carbon material at elevated temperature [18]. Meanwhile, indirect fluorination involves thermal decomposition of a fluorine source such as xenon fluoride (XeF_2) or terbium fluoride (TbF_4) in close proximity to the target carbon material [19-21]. Alternatively, functionalization of carbon materials can be achieved via plasma treatment at room temperature in carbon tetrafluoride gas (CF_4) [14,22-26]. Finally, chemical functionalisation can be achieved via e.g. alkyl fluorination [27,28].

The properties of the resulting fluorinated carbons depend not only on the type of carbon precursor, but also on the fluorination conditions, such as the duration of the reaction, the reaction temperature, the reaction pressure, and the type of fluorine-containing precursor [29]. Depending on these parameters, the C–F bonds which are generated during the reaction can be classed as ionic, semi-ionic, or covalent [30]. Previous studies have reported that when the proportion of fluorine atoms in fluorinated graphite is small (e.g. $x < 0.5$ in CF_X), ionic C–F bonds are generated, resulting in relatively high electronic conductivity [30]. However, when the concentration of fluorine atoms increases, covalent bonds are reported to form, resulting in decreased electronic conductivity due to the formation of sp^3 bonds [30]. As such, different

* Corresponding author at: Next-Generation Fuel Cell Research Center (NEXT-FC), Kyushu University, 744 Motooka, Nishi-ku, Fukuoka 819-0395, Japan.
E-mail address: can@kyudai.jp (E.M. Can).

https://doi.org/10.1016/j.apsusc.2023.157136
Received 20 December 2022; Received in revised form 12 March 2023; Accepted 24 March 2023
Available online 26 March 2023

Table 1
Summary of the fluorotelomer alcohol precursors used in this study.

Sample Name	Precursor Molecule	Precursor Structure	Boiling Point (Melting Point) (°C)	Fluorine Content in Precursor (at.%)
CF_x-C_{10}	Perfluoro-1-decanol ($C_{10}H_5F_{17}O$)	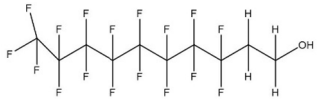	113 (50)	69.6
CF_x-C_8	Tridecafluorooctan-1-ol ($C_8H_5F_{13}O$)		88 to 95	67.8
CF_x-C_6	Perfluorohexan-1-ol ($C_6H_5F_9O$)	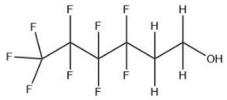	140 to 143	64.8
CF_x-C_5	Octafluoro-1-pentanol ($C_5H_4F_8O$)	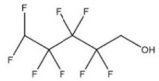	141 to 142	65.5

applications for fluorinated carbons may require different degrees of fluorination [1,5]. Moreover, for lithium batteries high fluorine content is preferred because C–F bonds act as electroactive species during discharge [31].

As such, it is of interest to investigate fluorinated carbons in which the amount of fluorine can be tailored to suit different applications. Several studies have focused on the effect of the fluorination parameters on the properties of the resulting fluorinated carbon materials [17,29,32,33]. Thermal annealing has been applied to different type of fluorinated carbons to gain insight into the stability of these materials. A high proportion of fluorine atoms in fluorinated graphene can be removed at mild temperatures under the inert atmosphere, but for complete removal a temperature higher than 500 °C is reported to be required [34,35]. The defluorination of carbon nanotubes has also been investigated, and it was found that single-wall carbon nanotubes fluorinated in F_2 (g) at 250 °C, were completely defluorinated at 400 °C under inert atmosphere [36].

In previous studies we have investigated the use of microporous carbon foams in energy applications. These foams are synthesized via thermal decomposition of sodium ethoxide, during which the precursor melts and the decomposition gases generate micron-scale pores via self-blowing. Meanwhile, micropores are generated via activation in the presence of the generated sodium hydroxide. We confirmed that these carbon foams are potentially useful in hydrogen storage applications due to their large surface area [37-39], or as catalyst supports [40,41].

Furthermore, nitrogen-doped carbon foams can be synthesized by reacting sodium metal with a mixture of ethanol and e.g. triethanolamine to generate a nitrogen-containing alkoxide intermediate product, followed by thermal decomposition in inert atmosphere [42-44]. These nitrogen-doped carbon foams have been applied as non-precious catalysts for the oxygen reduction reaction in polymer electrolyte fuel cells (PEFCs) [42], and metal-free catalysts for the CO_2 reduction reaction [45].

This method was then further modified, resulting in a completely new and relatively simple method for the synthesis of fluorinated carbons. Sodium was directly reacted with 2-perfluorohexyl ethyl alcohol in a sealed PTFE crucible, and the exothermic decomposition reaction generated superhydrophobic fluorinated carbon nanoparticles [9]. More recently, we applied these materials as alternative microporous layers in PEFCs, resulting in dramatically enhanced performance at high current density due to the improved water repelling properties [7].

The fluorine precursor used in the above works is a fluorotelomer alcohol (FTOH). The naming of these molecules commonly depends on the number of carbons which are fluorinated versus those that bond with hydrogen atoms. As such the 2-perfluorohexyl ethyl alcohol used above can be abbreviated to *6:2 fluorotelomer alcohol*. Fluorotelomers are generally used in the production of polyfluorinated alkyl substances (PFAS) which is used in fire-fighting foams, grease-resistant papers, anti-fogging sprays and wipes [46].

Here, we further investigate this unique solvothermal method for the synthesis of fluorinated carbon. Specifically, the effect of using different fluorotelomer alcohol precursor molecules is examined, with new insights into the microstructure and chemical structure of the resulting carbons.

2. Experimental

All chemicals were used as received from suppliers without further purification. Four fluorotelomer alcohols with different chain length were utilised as precursors for fluorinated carbon synthesis, namely: (i) perfluoro-1-decanol ($C_{10}H_5F_{17}O$, Fluorochem, Ltd. Japan); (ii) tridecafluorooctan-1-ol ($C_8H_5F_{13}O$, Funakoshi Co., Ltd., Japan); (iii) perfluorohexan-1-ol ($C_6H_5F_9O$, Sigma Aldrich, Japan); and (iv) octafluoro-1-pentanol ($C_5H_4F_8O$, Sigma Aldrich, Japan). 0.022 mol of each respective fluorotelomer alcohol was pipetted into 100 ml polytetrafluoroethylene (PTFE) crucibles (Flon Industry, Japan), followed by the addition of 0.088 mol of metallic sodium lumps under flowing nitrogen. The PTFE crucible was quicky sealed, and then screwed into a protective stainless steel jacket. This was placed into a preheated oven at 150 °C for 24 h, then cooled naturally to room temperature.

After cooling, the stainless steel jacket was carefully unscrewed in a well-ventilated fume hood, taking precautions for the possible presence of hydrogen fluoride fumes. The black powdery product was emptied into a two-liter glass beaker filled with a 50:50 vol% mixture of deionized water and ethanol, sonicated for one hour, and then stirred at 1000 rpm for 24 h. The dispersion was then washed by vacuum filtration using Omnipore^{TM} 0.2 μm filters until the filtrate reached neutral pH. Finally, the resulting black powder was dried in a convection oven at 65 °C for 24 h. Detailed information about the reactions are presented in Table 1. The samples are named as CF_X-C_N. CF_X indicates that the sample is fluorinated carbon where C_N is the number of carbon atoms in the precurser that was used to synthesis of fluorinated carbon. For example, CF_X-C_{10} corresponds to fluorinated carbon synthesised using perfluoro-1-decanol ($C_{10}H_5F_{17}O$), which contains 10 carbon atoms in its structure.

The fluorinated carbon products were characterized by field emission scanning electron microscopy and energy dispersive X-ray analysis (FE-SEM EDX, SU9000, Hitachi); transmission electron microscopy (TEM, Titan^{TM} ETEM G2, FEI Company); X-ray photoelectron spectroscopy (XPS, PHI 5000 Versa probe (II) ULVAC); nitrogen adsorption analysis (Belsorp Mini X, Microtrac MRB); X-ray diffraction analysis (λ = 1.54 Å, SmartLab 9kw AMK, Rigaku); thermogravimetric analysis (TGA, Rigaku Themo plus EV02); and Raman spectroscopy (λ = 532 nm,

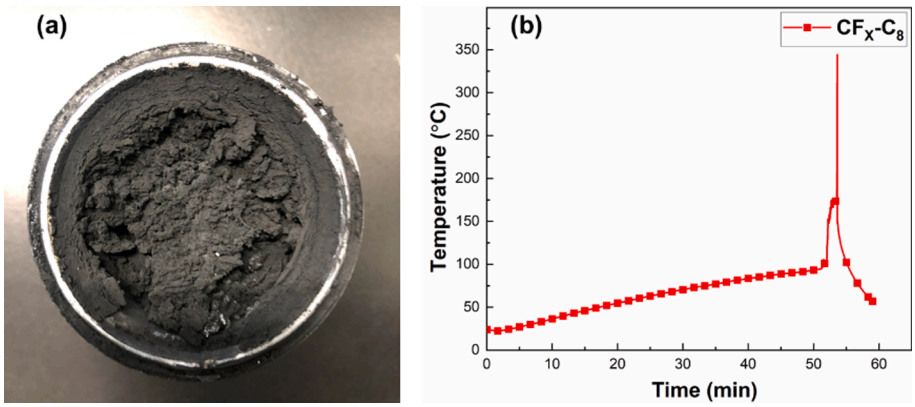

Fig. 1. (a) Photograph of sample CF_x-C_8 immediately after opening the PTFE reactor. (b) Plot of the temperature inside the PTFE crucible during the reaction.

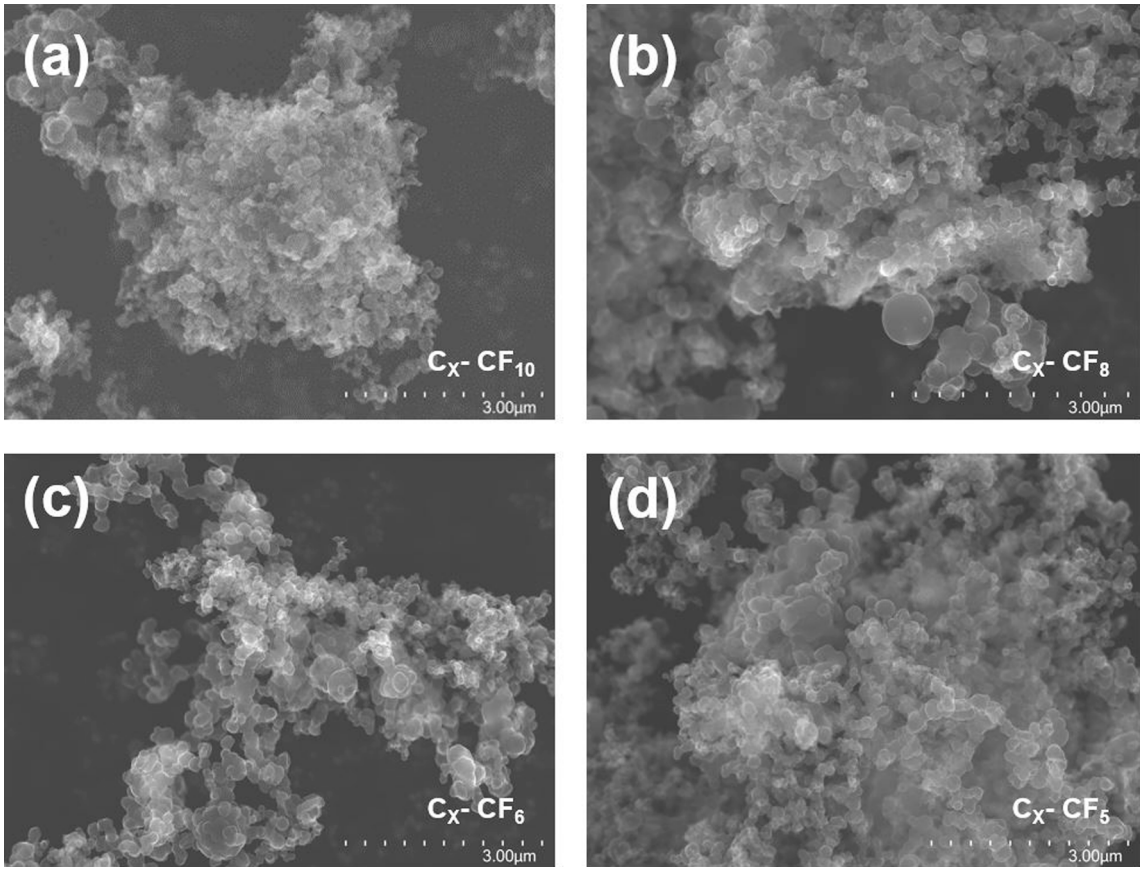

Fig. 2. SEM images of the four fluorinated carbons synthesized in this work: (a) C_X-CF_{10}; (b) C_X-CF_8; (c) C_X-CF_6; and (d) C_X-CF_5.

inVia Raman Microscope, Renishaw). The apparent water contact angle (WCA) was measured using the sessile drop method with an automated surface measuring instrument (DMs-401, Kyowa Interface Science Co., Ltd, Japan). Fluorinated carbon powders were pressed between two glass slides to form a smooth surface. The droplet size was set to 1 µL.

3. Results and discussion

On removal from the PTFE reactor, the superficial appearance of the product was similar regardless of which fluorotelomer alcohol was used as a precursor during synthesis. All four of the generated samples were observed to be a fine dry black powder, mixed with a small amount of white residue (Fig. 1a, Fig. S1). This white residue has been identified in our previous works as sodium fluoride (NaF) [7,9], and this was largely removed during the washing stage. A speculative non-stoichiometric scheme for this decomposition reaction is given as follows:

$$CF_3(C_7F_{14})C_2H_2OH + Na \rightarrow CF_x + NaF + HF + NaO(H) \quad (1).$$

After the reaction the PTFE crucible was discolored and slighly deformed. This suggests that the reaction temperature exceeded the softening point of PTFE (250 °C) despite the oven temperature being just 150 °C, i.e. that the process was exothermic. To confirm this, the progression of the reaction temperature inside the PTFE crucible was recorded using a thermocouple for sample CF_X-C_8. Only this sample was measured due to safety considerations when using the thermocouple during this experimental set-up. This data (Fig. 1b) shows that the temperature steadily increased for 52 min after the reactor was placed in the oven, towards the target temperature of 150 °C. However, when the internal temperature reached 102 °C, a rapid increase in temperature

was observed, reaching 345 °C in less than a minute. After a maximum in temperature was observed, the oven was turned off and the vessel is observed to quickly cool to <150 °C after this. This data confirms that the reaction between sodium and tridecafluorooctan-1-ol is highly exothermic, and that the reaction occurs relatively quickly.

The mass yields were calculated for the four different samples, which were 34, 29, 18 and 32 % for CF_X-CF_5, CF_X-C_6, CF_X-C_8, and CF_X-C_{10}, respectively, relative to the initial mass of the fluorotelomer precursors. The yields do follow any obvious trends, but may be due to different temperatures achieved during the reactions, or loss of product during sample washing.

Considering the high temperature achieved, and the observed damage to the PTFE vessel, scale up could be challenging. However, there is the possibility to use more thermally resiliant reaction vessels, such as graphite, or ceramic coated chambers. Furthermore, nanodiamonds are currently synthesized at scale by detonation-synthesis, and the high temperature and high pressure reaction vessels used for that reaction may also be appropriate.

The microstructure of the four different fluorinated carbon products was first investigated by SEM (Fig. 2). Each sample is comprised almost entirely of spheroidal nanoparticles with similar structure to that of carbon black. These are clustered together in loosely aggregated structures several microns across, leaving micron-scale voids. Some larger wall-like structures are also observed in some regions of the sample, but with extremely low occurrence (Fig. S2). The SEM images clearly indicate that the diameter of the primary nanoparticles mainly varies between 50 and 100 nm for all four samples, although occasionally much larger micron-scale particles are also observed (Fig S3). The use of dynamic light scattering to determine primary particle size was not possible due to the highly hydrophobic nature of the materials and aggregation preventing their dispersion in water. It may be of interest in future to explore dispersion in alternative solvents to determine a more accurate estimate of primary particle size.

The spherical structure of the nanoparticles strongly suggests that they are formed from liquid droplets, the shape being driven by surface tension. This would be analogous to the synthesis of carbon black, in which a liquid hydrocarbon precursor is injected into a high temperature reaction vessel as an atomized aerosol, after which it forms spheroidal carbon particles via incomplete combustion. In the case of these fluorinated carbons, we propose that the precursors enter a supersaturated mixed state within the PTFE vessel, forming suspended droplets which then decompose to form the observed spheroidal nanoparticles. This is supported by the fact that the boiling point of tridecafluorooctan-1-ol is around 95 °C, which is very close to the temperature at which the reaction is observed to proceed.

All four samples have similar microstructure and particle size distribution, regardless of the fluorotelomer precursor used. It is unclear at present why this is, but it may be related to the surface tension of precursors after they melt in the reactor, since surface tension dictates the droplet size of liquids. The intermolecular bond strength is likely similar between the different fluorotelomers, leading to similar surface tension and ergo similar droplet size. This result also confirms for the first time that this novel synthetic process is repeatable and can be generalized to different precursors.

Nitrogen adsorption/desorption isotherms of all the fluorinated carbon samples were recorded to provide insight into the microstructure (Fig. S4). Brunauer-Emmett-Teller (BET) and Barrett-Joyner-Halenda (BJH) methods were used to estimate the specific surface area and pore size distributions from the isotherms. The specific surface areas of CF_X-C_{10}, CF_X-C_8, CF_X-C_6, and CF_X-C_5 were measured to be 25.6, 27.6, 25.7 and 26.6 m^2/g, respectively, which are surprisingly low values for carbon nanomaterials. BJH and micropore (MP) plots show that these fluorinated carbons have very low mesopore volume and micropore volume, whilst the small pore volume observed can probably be attributed to the spaces between the particles observed by SEM, rather than being inherent to the nanoparticles themselves. All four samples display Type III isotherms, which are characteristic of non-porous materials [47].

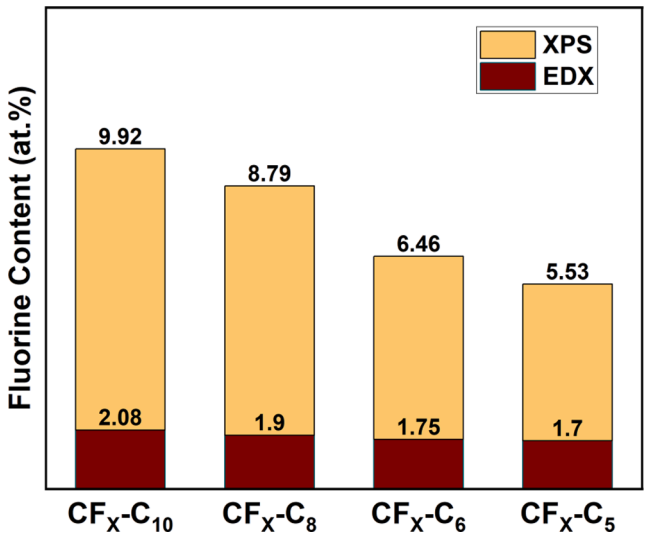

Fig. 3. Fluorine content as measured by XPS and EDX.

Overall, the surface area and pore volumes are much lower compared to the non-fluorinated porous carbons prepared in a similar manner and previously reported by our group [37,38,44,48]. In those cases, the high surface area and porosity is attributed to the formation of sodium hydroxide (NaOH) during synthesis, which acts as an activation agent to generate micro- and mesopores. However, in the case of fluorinated carbon synthesis, this activation evidently does not occur. This could be attributed (i) to the high proportion of sodium fluoride (NaF) which is preferentially formed, decreasing the amount of NaOH activation agent present in the sample, or (ii) to the lower synthesis temperature in this case (activation is generally held to occur at >500 °C). Meanwhile, (iii) differences in pressure within the PTFE crucible and the viscosity of the melting precursors as they decompose may also be a factor. Furthermore, (iv) fluorination has been previously reported to decrease surface area and pore volume by blocking micropores [30].

The elemental compositions of the synthesized carbons as determined by XPS are shown in Table S1, and the corresponding fluorine contents are plotted in Fig. 3. The results confirm that all the carbon samples contain a significant amount of fluorine. In addition, *the amount of fluorine detected in the samples correlates strongly with the proportion of fluorine in the fluorotelomer alcohol precursor*, ranging from 5.5 at.% for CF_X-C_5 to 9.9 at.% for CF_X-C_{10}. These values are reasonable considering that fluorographene reportedly has a C:F ratio of 1:1 [49]. Meanwhile, the oxygen content varies between 1.4 at.% and 2.1 at.% for all samples, and trace quantities of sodium are found, attributed to small amounts of remaining sodium fluoride. This NaF may be encapsulated within the samples, rendering it inaccessible during the washing step.

Fig. 4 shows the XPS survey and narrow scans for CF_X-C_{10}, whilst CF_X-C_5, CF_X-C_6, and CF_X-C_8 are shown in Figs. S5, S6 and S7 respectively. Whilst the amount of fluorine varies depending on the type of fluorotelomer alcohol precursor, the narrow scan and deconvoluted spectra have remarkably similar profiles. This confirms the reproducibility of this synthesis method even when different precursors are used. Previously, it has been reported that either ionic or covalent C–F bonds can be formed depending on the fluorination conditions, namely ionic bonds for low fluorine content, semi-ionic for mild fluorination, and covalent bonds for harsher fluorination conditions [1]. The binding energy of semi-ionic C–F bonds is generally assigned to around 287 eV in the C 1s region, and around 685.5 eV in the F 1s region [30]. For covalent C–F bonds, the binding energy is reported to depend on the amount of fluorine, varying between e.g. 289 eV for CF and 290.2 eV for CF_2 in the C 1s region, and around 688 eV in the F 1s region [50]. Furthermore, due

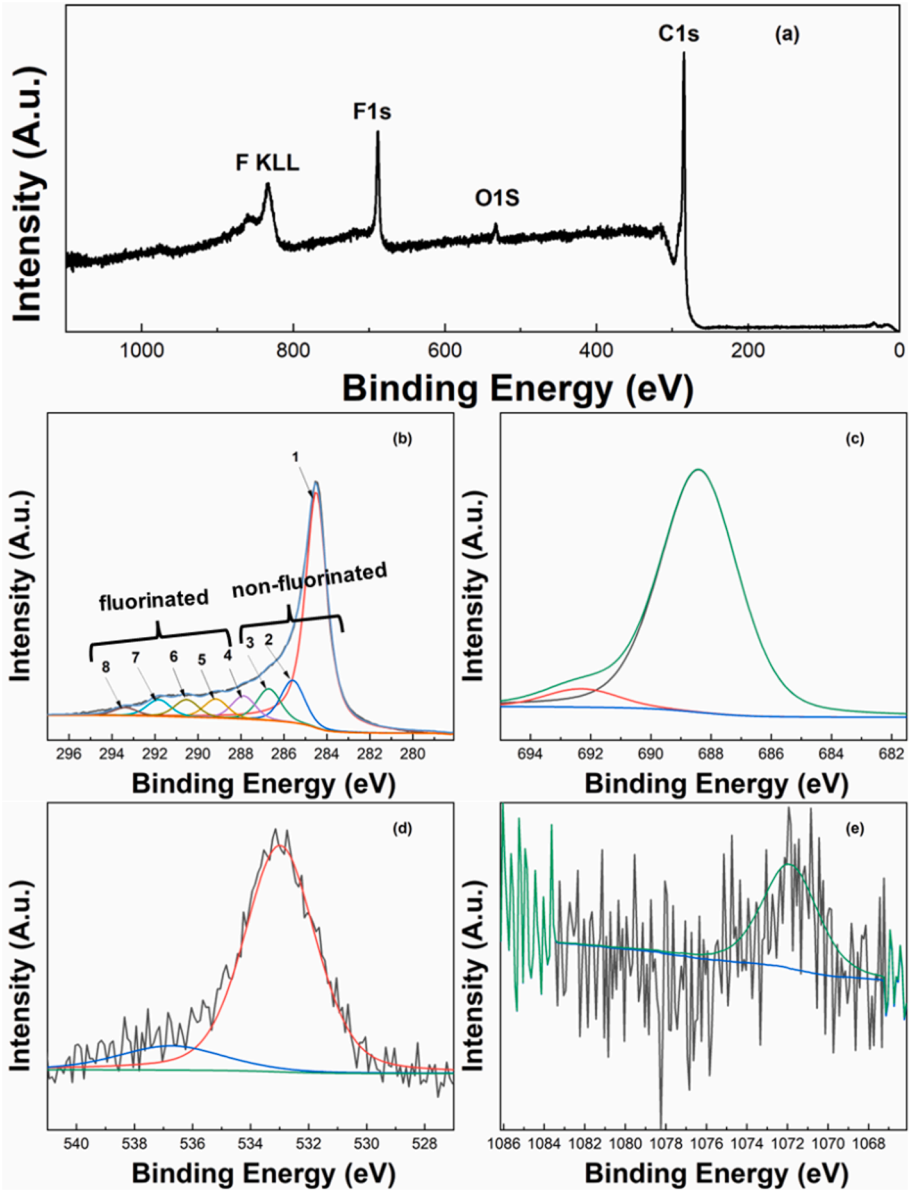

Fig. 4. XPS of CF_X-C_{10}: (a) survey spectrum; (b) C 1s region, (c) F 1s region; (d) O1s region; and the (e) Na 1s region.

to the high electronegativity of fluorine atoms, charging is expected to shift the spectra to slightly higher binding energy [9].

Fig. 4(b) shows the C1s region deconvoluted into different contributions. Peaks at (1) 284.5 eV, (2) 285.6 eV, and (3) 286.7 eV are assigned to sp^2 bonding, sp^3 bonding and C-O bonds, respectively [10]. Meanwhile, the component at (4) 288 eV is attributed to C–F bonds at structural defects, and/or at the periphery of graphitic domains [50]. The component at (5) 289.1 eV is assigned to covalent C–F bonds at the alpha position in border CF_2 groups [50], and the component at (6) 290.2 eV is assigned to border CF_2 and CF groups surrounded by other CF groups [10]. Finally, the components at (7) 291.8 eV and (8) 293.5 eV are assigned to perfluorinated groups [9]. The F1s region (Fig. 4c) is deconvoluted into two peaks at 688.4 eV and 692.4 eV which are assigned to covalent C–F bonds [51-55]. Finally, the O1s region in Fig. 4d has a broad signal centred at 533 eV, corresponding to C-O bonds. A small shoulder is observed at 536 eV corresponding to the sodium auger peak (Na KLL). No significant signals are observed at lower binding energy in the F1s region (e.g. <686 eV), suggesting that fluorine atoms are covalently bonded to carbon rather than ionically bonded.

Table S2 shows the elemental composition of the samples as measured by EDX. In this case, the elemental composition of all the samples is similar. The carbon contents vary between 89 and 93 at.%, whilst the fluorine content remains between 1 and 2 at.% in all cases. The oxygen content varies from 5 to 9 at.%, and trace amounts of sodium are detected. Similar to the case of XPS, EDX show that the fluorine content of the product is proportional to the amount of fluorine in the fluorotelomer alcohol precursor. However, the atomic concentration of fluorine (1 to 2 at.%) is much lower than that measured by XPS (i.e. 5 to 9 at.%). This discrepancy is attributed to the fact that XPS is a quasi-surface sensitive analysis technique with a penetration depth of just ~5 to 10 nm, whilst EDX is a bulk measurement technique with a much greater penetration depth of 1 to 2 μm. Therefore, the difference in measured values suggests that fluorination mostly occurs near the surface of the carbon. As such, XPS detects a higher fluorine content concentrated near the exposed surface of the carbon, whereas EDX records the average fluorine content throughout the whole sample, which includes the unfluorinated core of the particles.

Furthermore, the oxygen content of the samples is significantly higher according to EDX (i.e., 6 to 7 at%) compared to that measured

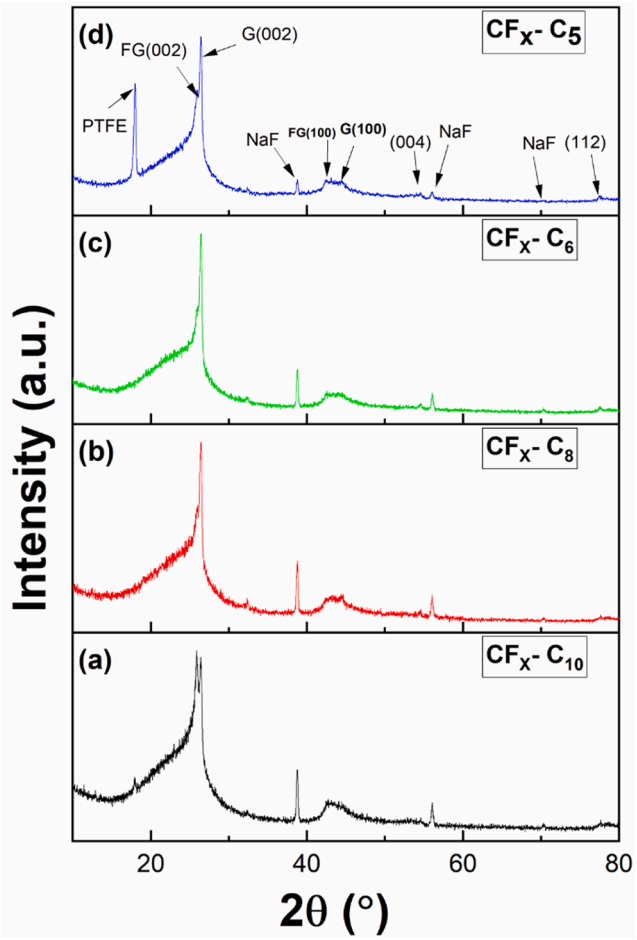

Fig. 5. XRD for the four fluorinated carbon samples: (a) C_X-CF_{10}; (b) C_X-CF_8; (c) C_X-CF_6; and (d) C_X-CF_5.

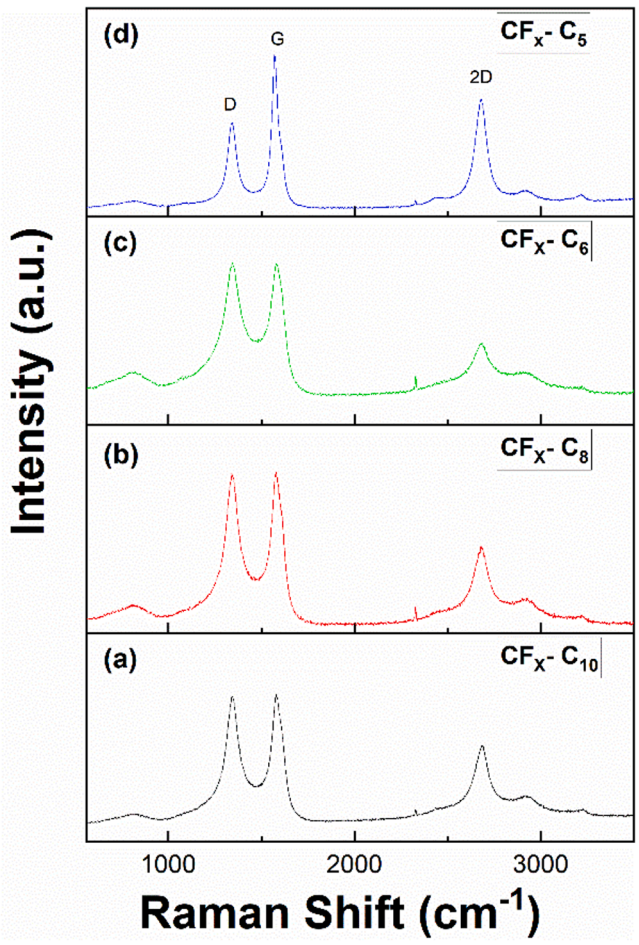

Fig. 6. Raman spectroscopy of the fluorinated carbon samples: (a) C_X-CF_{10}; (b) C_X-CF_8; (c) C_X-CF_6; and (d) C_X-CF_5.

using XPS (i.e. 1 to 2 at.%). Using the same reasoning, this might suggest that oxygen is not as highly concentrated at the surface. Conventional carbon nanomaterials can be relatively hydrophilic, and thus XPS tends to detect a high concentration of oxygen atoms due to adsorbed water molecules on the surface. However, fluorinated carbon materials are generally hydrophobic, and thus water adsorption is not expected to be significant. The oxygen atoms detected here using EDX could be associated with e.g. residual sodium hydroxide encapsulated within the material and therefore protected from the washing step. Fig. S8 shows representative EDX mapping of sample CF_X-C_6. The presence of fluorine is confirmed throughout the whole structure, indicating that the sample is uniform. Meanwhile, in some areas, fluorine and sodium signals have high intensity and overlapping EDX signals, strongly indicating the presence of small amounts of sodium fluoride. It is likely that this sodium fluoride is encapsulated within the fluorinated carbon particles, preventing it from being removed during the washing step, as also observed in our previous studies [7,9].

The crystallographic structure of the synthesized fluorinated carbons was investigated using XRD (Fig. 5). In all samples, similar peaks positions are observed, although there are some clear differences in the relative peak intensities. In some samples, a diffraction peak is observed at 18 ° (equivalent to a lattice spacing of 0.49 nm). This peak corresponds closely to crystalline PTFE [56]. As such, this indicates contamination of the sample from the PTFE reaction vessel. Indeed, as shown in Fig. 1b, the reaction temperature briefly exceeded the melting point of PTFE and discoloration was observed. As such there is a possibility that some of the material from the vessel walls was transferred to the carbon sample, resulting in this XRD peak. This peak has the highest intensity for sample CF_X- C_5, which may indicate that a higher temperature was reached (although this is yet to be confirmed). This may be because CF_X-C_5 has the shortest chain length, leading to more exothermic (and/or less endothermic) decomposition reactions.

Two narrow peaks are also observed at 25.9 ° and 26.4 °, corresponding to lattice spacings of 0.342 and 0.337 nm, respectively. The later of these corresponds very closely with the lattice spacing of graphite (0.336 nm). Meanwhile, the former could be attributed to the 002 planes of surface fluorinated carbon and/or amorphous carbon due to the introduction of sp^3 bonds to the graphitic system. Furthermore, the crystallite size of the graphitic carbon phases in each sample were calculated using the Scherrer equation on the 002 peak. These were found to be 36.3, 26.6, 30.5, and 31.8 nm for CF_X-C_{10}, CF_X-C_8, CF_X-C_6, and CF_X-C_5, respectively. Similarly, two separate peaks are observed at 42.8 ° and 44.5 °, corresponding to lattice spacings of 0.211 and 0.203 nm and attributed to the 100 planes of fluorinated carbon and graphitic carbon [6,31,32]. Previous studies have shown that the interlayer spacing of graphite increases due to fluorination, because of an increase in sp^3 type bonding [30,57-59]. In addition, two more carbon related diffraction peaks with much smaller intensity were observed at 54.5° and 77.5°, corresponding to lattice spacings of 0.168 and 0.123 nm, respectively. These are assigned to the 004 and 112 crystal planes of graphitic carbon. Finally, three very small diffraction peaks are observed at 38.8, 56.0, and 70.3°, which are attributed to the 200, 220, and 222 crystal planes of sodium fluoride [60].

Raman spectroscopy was used to further probe the chemical structure of the synthesized carbons (Fig. 6), and the spectra strongly resemble those of graphitic materials commonly reported in the

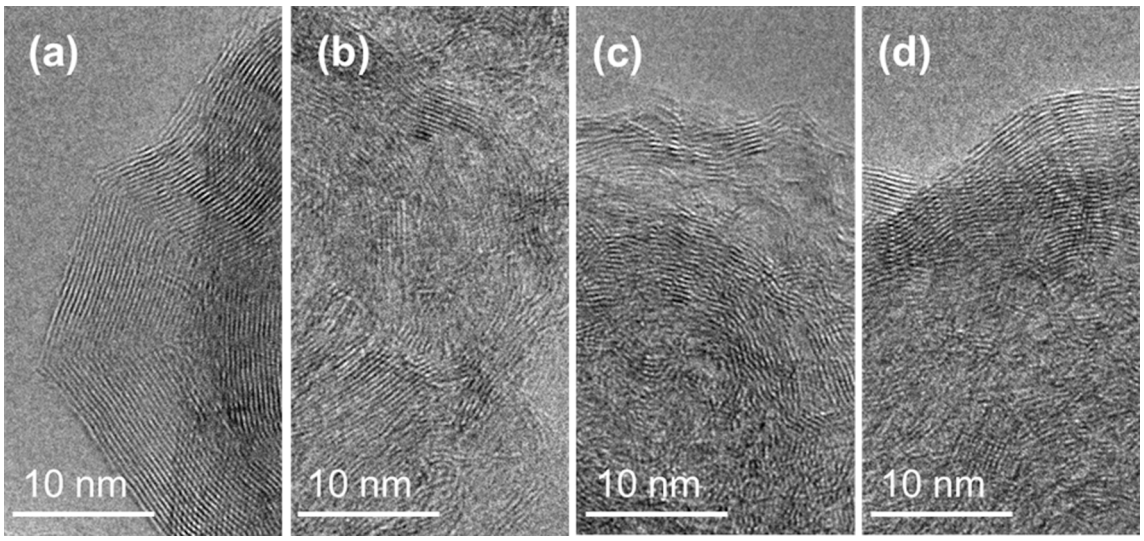

Fig. 7. TEM images of the fluorinated carbon samples: (a) C_X-CF_{10}; (b) C_X-CF_8; (c) C_X-CF_6; and (d) C_X-CF_5.

literature [61,62]. The most prominent features in the Raman spectra of graphitic materials are the G band at ~1582 cm^{-1} and the D band at ~1350 cm^{-1}, as well as the D' band at ~1620 cm^{-1} and the 2D or G' band at ~2700 cm^{-1}. The G band is associated with the structural intensity of the sp^2-hybridized carbon atom. The D band is generally associated with defects graphitic (sp^2) carbon, and it has been reported that the intensity of this peak can increase due to the sp^3 bonding of fluorine in graphene [63].

In all the fluorinated carbon samples, the D band is centred at ~1342 cm^{-1} has a relatively high intensity, which is attributed directly to the fluorine content. The G peak is centred at 1580, 1578, 1579, and 1571 cm^{-1} for CF_X-C_{10}, CF_X-C_8, CF_X-C_6, and CF_X-C_5, respectively. The shifting of the G peak is attributed to the different layer thicknesses of the graphitic structure and/or the fluorine doping [61]. Meanwhile, the ratio of the intensity of the D and G bands is commonly used to estimate the density of defects in the structure. In this case, the I_D/I_G values are 0.99, 0.99, 1.00, and 0.56 for CF_X-C_{10}, CF_X-C_8, CF_X-C_6, and CF_X-C_5, respectively. The lower ratio for CF_X-C_5 suggests a lower degree of disorder, as discussed below, whilst values close to 1 are typical for amorphous carbons synthesized from metal alkoxides [48]. Furthermore, the 2D peak observed at ~2680 cm^{-1} has a profile similar to that of bulk graphite [62]. Between the D and G bands a relatively high signal intensity is observed for all samples, which is referred to as the D3 band in the literature. Previous studies suggest that this D3 band originates from the amorphous carbon fraction in the structure [64]. The D3 band signal intensity varies between samples. The lowest intensity recorded for sample CF_X-C_5 which indicates the relatively smaller amount of amorphous region compared to other 3 samples.

The highest intensity of the XRD diffraction peak at 25.9° (corresponding to surface-fluorinated graphite) was obtained for sample CF_X-C_{10}. This is in agreement with the elemental analysis, which showed that this sample has the highest fluorine amount, of 9.9 at. %. Meanwhile, the diffraction peak at 18° (corresponding to PTFE) has the highest intensity for sample CF_X-C_5. This may indicate that this sample contains a higher degree of PTFE contamination. In addition, this same sample had the lowest intensity D peak in the Raman spectra, indicating that this is the most graphitic of the samples, and it also had the lowest fluorine content (5.5 at.%). These factors combined strongly suggest that this sample reached a higher reaction temperature than the other three samples.

The local crystal structure was examined in more detail using TEM and SAED. The TEM images (Fig. 7) clearly reveal the presence of highly graphitized carbon with well-defined crystal structure, for all four of the samples. The graphitic structure appears to be more prominent near the outer surface of the particles, whilst the interior contains more amorphous regions. This mixture of different crystallographic phases may explain the combination of the highly developed 2D peak in the Raman spectra in combination with the large D peak. Meanwhile, the SAED results confirm the crystalline nature of the fluorinated carbon samples, with prominent diffraction rings corresponding to the 002, 101, 004, and 112 planes of graphitic carbon (Fig. S9).

Taken as a whole, the XPS, XRD, Raman and TEM data results discussed above suggest that the fluorinated carbon materials in this work are made up of amorphous carbon, fluorinated carbon, and graphitic regions. We suggest that the core of the nanoparticles is mainly composed of relatively amorphous carbon, whilst both fluorinated carbon and highly graphitised carbon phases exist near the surface.

The fluorinated carbons synthesized in this work clearly include highly graphitic regions. This is despite the relatively low temperature used during the solvothermal reaction (namely, 150 °C). Even considering the exothermic nature of the reaction, the temperature inside the vessel only increased to ~350 °C according to Fig. 1. Under normal circumstances, the synthesis of graphitic carbon requires the application of very high temperatures. For example, graphitization of carbon is typically performed at temperatures of >3000 °C [65]. Alternatively, carbon nanotubes are highly graphitic and are synthesized at intermediate temperature (e.g. 650 °C), but the graphitization in this case is assisted by the presence of a transition metal catalyst, usually in the form of iron, cobalt or nickel nanoparticles [66]. However, the solvothermal synthesis of fluorinated carbons from sodium and fluorotelomer alcohol precursors takes place in a PTFE vessel without exposure to conventional catalysts. Furthermore, the non-fluorinated carbons synthesized in our group using similar methods and identical equipment are not only highly amorphous, but remain so even at pyrolysis temperatures up to 1400 °C [37,42].

As such, the mechanism behind the formation of highly graphitised regions in these fluorinated carbons is unclear. The recorded reaction temperature is much lower than that usually required for graphitisation, and there is no indication of the presence of transition metal catalyst particles such as iron or cobalt. Instead, we propose for the first time that HF molecules briefly generated during the decomposition of the fluorotelomer alcohol have a catalytic effect, aiding in the formation of graphitic C–C bonds at high temperature and pressure. Indeed, HF-assisted alkylation is commonly used in gasoline production, in which low-molecular-weight alkenes are converted into alkylate via carbon–carbon bond formation [67-69]. This is supported by the observation that the interior of the nanoparticles is more amorphous, whilst the outside graphitic, which can be attributed to the outer surface of the particle being exposed to HF for longer periods of time, producing a

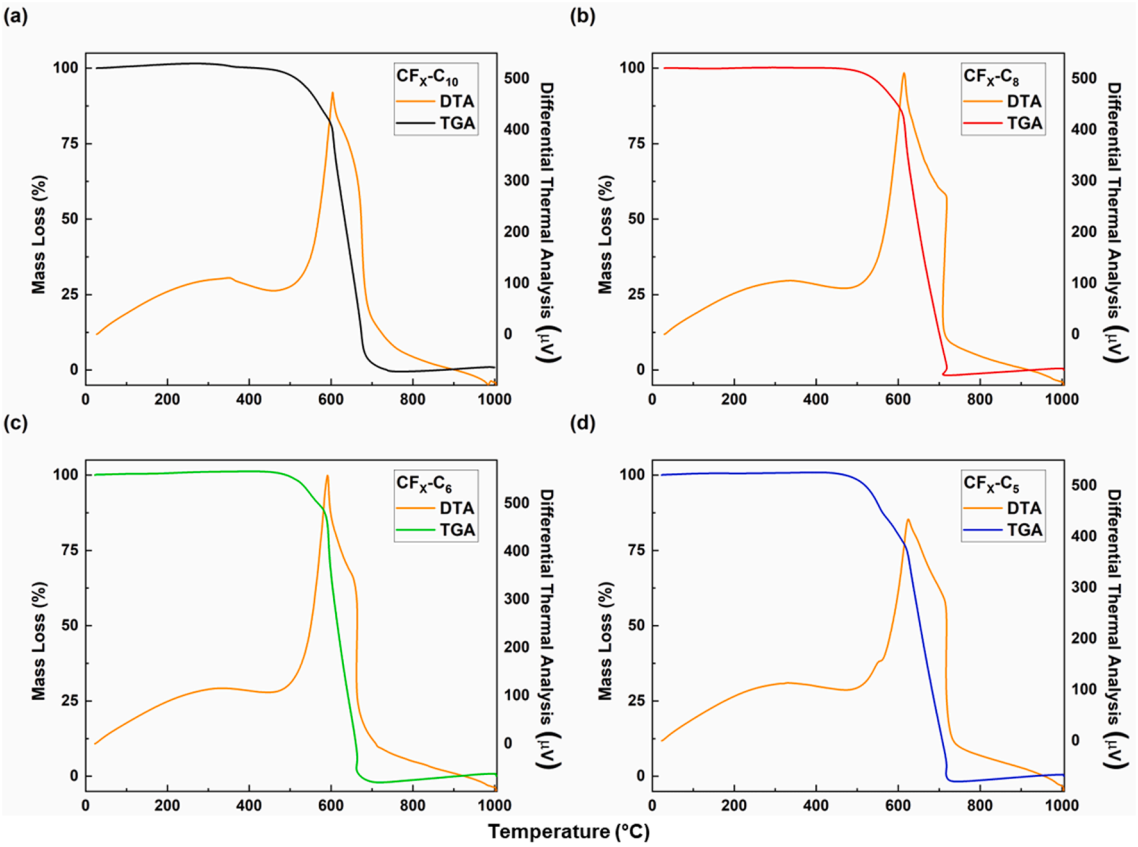

Fig. 8. Thermogravimetric analysis (TGA) and differential thermal analysis (DTA) of the synthesized fluorinated carbons: (a) C_X-CF_{10}; (b) C_X-CF_8; (c) C_X-CF_6; (d) C_X-CF_5.

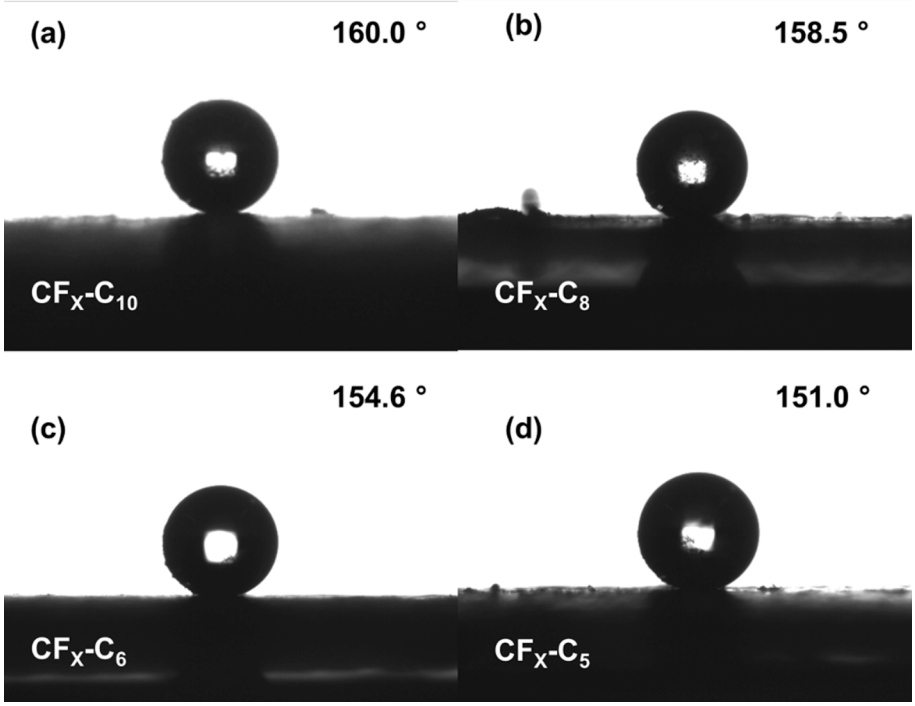

Fig. 9. Water contact angle (WCA) measurements for: (a) C_X-CF_{10}; (b) C_X-CF_8; (c) C_X-CF_6; (d) C_X-CF_5.

greater degree of graphitization. This mechanism will be further investigated in future work.

Subsequently, the thermal stability of the synthesized fluorinated carbons was investigated using thermogravimetric analysis (TGA) and differential thermal analysis (DTA) in flowing air (Fig. 8). Differential thermogravimetry (DTG) is shown in Fig. S10. All four samples display

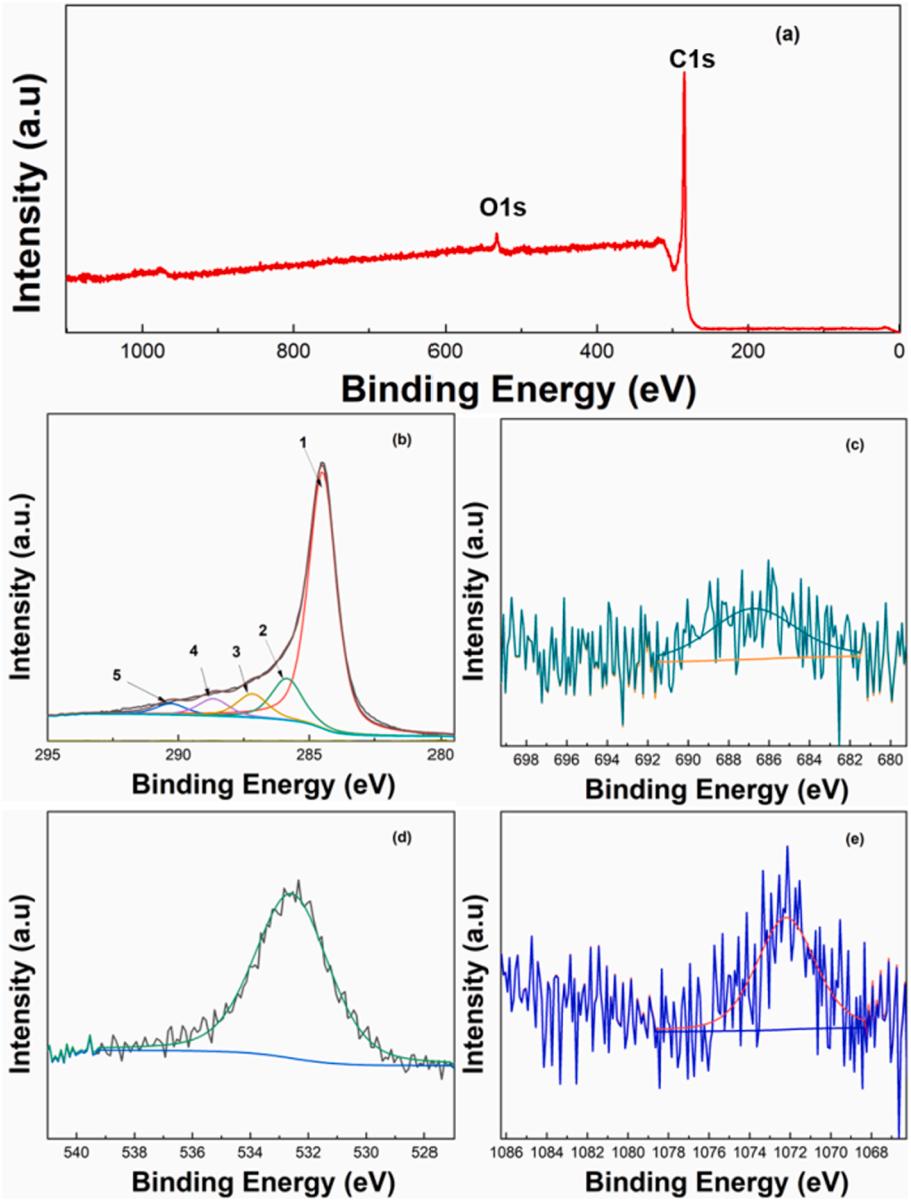

Fig. 10. XPS of CF_X-C_8-HT: (a) survey spectrum; (b) C 1s region; (c) F 1s region; (d) O1s region; and (e) Na 1s region.

similar profiles and are thermally stable up to ~500 °C. The first mass loss is attributed to the breaking of C–F bonds, manifesting as a slow decrease in the TGA curve and a small local minimum in the DTG at ~580 °C. When the temperature reaches ~600 °C, a rapid exothermic mass loss is observed representing reaction between carbon and oxygen in the air. The samples were completely consumed once the temperature reached ~700 °C in all cases.

Due to the low free energy of hydration and in combination with the large diameter of fluorine atoms (leading to low surface density and poorer van der Waals interactions with water [70]), fluorinated carbons are generally hydrophobic. This is also the case with the fluorinated carbons synthesised in this work. This is the reason for washing with an ethanol: water mixture, because pure water will not interact with the resulting carbon materials at all. The relative hydrophobicity of the carbons synthesised in this work was evaluated using the apparent water contact angle (WCA) averaged over 10 measurements (Fig. 9). The average apparent WCAs of C_X-CF_{10}, C_X-CF_8, C_X-CF_6, and C_X-CF_5 are 160.0°, 158.5°, 154.6°, and 151.0°, respectively. These results confirm that all of the synthesised samples display highly hydrophobic nature of the material. Furthermore, there is a clear trend in which higher fluorine content results in higher water contact angle. Importantly, this result shows that is possible to tailor the water contact angle of these fluorinated carbons by varying the type of fluorotelomer alcohol precursor, which could be important in e. g. electrochemical applications. For example, flooding is one of the major issues at the cathode side of the polymer electrolyte fuel cells (PEFCs), preventing oxygen from reaching the catalyst layer and strongly affecting performance at high current density. Creating electrodes with areas of both high and low hydrophobicity can improve oxygen transport by simultaneously providing water repelling gas transport regions as well as water wicking regions [71-73].

It has been previously reported that fluorine atoms can be removed from fluorinated graphene via thermal annealing [34,58]. To explore the effect of thermal treatment on these fluorinated carbons CF_X- C_8 was selected for a secondary heat treatment in a tube furnace at 700 °C (5 °C/min heating rate) under flowing nitrogen (100 ml/min), for one hour. The resulting sample is labelled CF_X-C_8-HT.

XPS analysis reveals that after secondary thermal treatment, CF_X-C_8-HT comprises 97.01 at.% carbon, 2.67 at.% oxygen, 0.16 at.% sodium and just 0.16 at.% fluorine (Fig. 10). This confirms that most fluorine

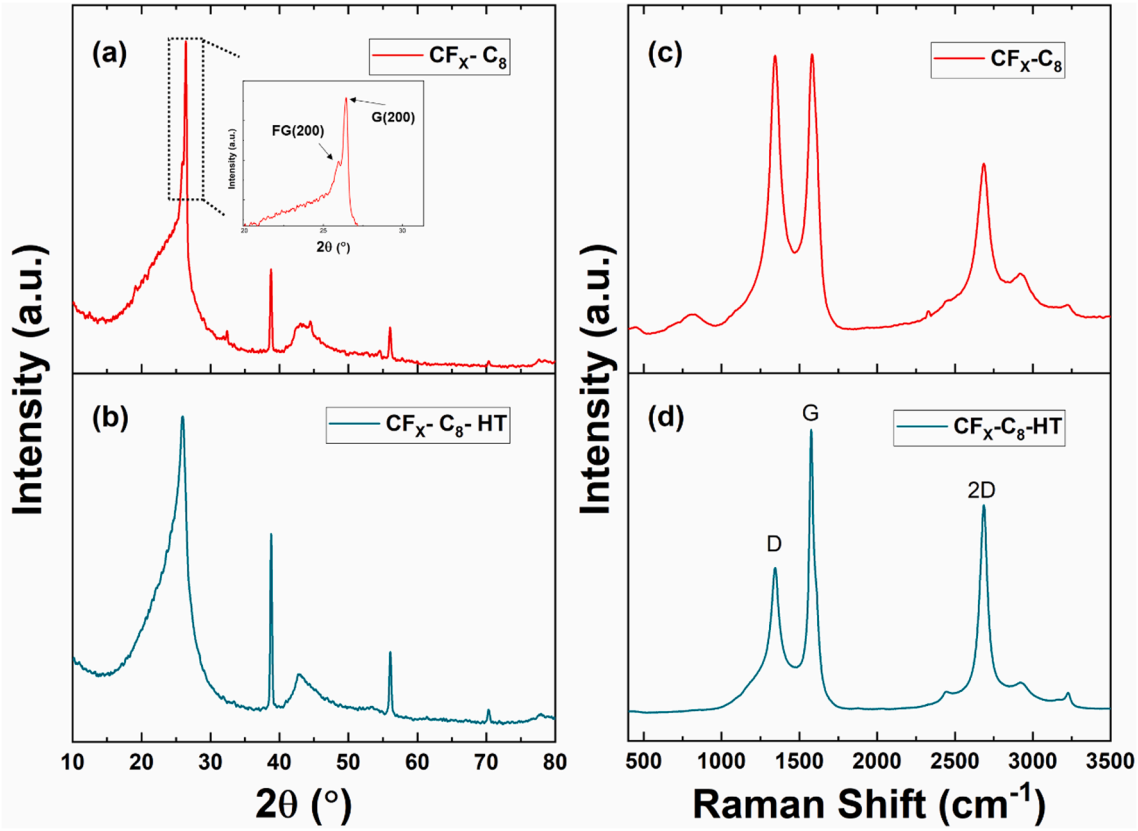

Fig. 11. (a-b) XRD and (c-d) Raman spectra of CF_X-C_8 and CF_X-C_8-HT.

atoms can be removed from the synthesized fluorinated carbons via thermal annealing. Since the concentration of sodium and fluorine are similar, the remaining fluorine atoms are likely in the form of encapsulated sodium fluoride, which is thermally stable with a melting point of 993 °C. The oxygen content of CF_X-C_8-HT is slightly increased compared to CF_X-C_8 (Table S1), which is attributed to an increased proportion of absorbed water vapor after heat treatment, due to loss of the hydrophobicity. The C1s region of CF_X-C_8-HT is deconvoluted into 5 main peaks, corresponding to (1) sp^2 carbon at 284.5 eV; (2) aliphatic sp^3 carbon at 285.6 eV; (3) C–O bonds at 286.7 eV; (4) O–C=O bonds at 288.5 eV; and (5) C1s shake-up. The small F1s peak at 687.5 eV and the Na1s peak at 1072 eV correspond to NaF.

To further clarify the effect of secondary thermal annealing, CF_X-C_8-HT was analysed by XRD (Fig. 11. (a-b). The diffraction peaks at 25.9, 42.8, 54.5 and 77.5 ° are assigned to the 002, 100, 004 and 112 crystal planes of graphite, respectively. Surprisingly, despite the removal of fluorine atoms during secondary thermal annealing, the wider d-spacing associated with surface-fluorinated graphite is retained (namely at 0.342 nm), whilst the narrower d-spacing associated with graphite is less prominent. This is contrary to reports in previous studies, in which the d-spacing of graphitic fluorinated carbons contracts upon the removal of fluorine atoms, reverting back to its graphitic form [58,74,75]. This effect may be related to the microstructure and chemical structure of the carbon under investigation. Like the case of non-graphitizable carbons [76], crosslinking of basic structural units in the structure, and/or interatomic corrugation, [35] may prevent contraction of the graphitic layers in this case, despite the removal of fluorine. Alternatively, this may be related to the presence of regions with different crystallographic order, with the lower order regions (i.e. more amorphous) being fluorinated more readily [77-79]. Meanwhile, peaks at 38.8, 56.0, and 70.3 ° are assigned to different orientations of crystalline NaF. The relative intensity of the peaks assigned to NaF increases significantly after the secondary thermal treatment. This increase in intensity is attributed to the fact that NaF has a melting point of 993 °C, and is therefore unaffected by secondary thermal treatment at 700 °C.

Raman spectra before and after secondary heat treatment are shown in Fig. 11. (c-d). After thermal annealing, the intensity of the D peak decreases dramatically, as also reflected by a significant decrease in the I_D/I_G ratio from 0.99 for CF_X-C_8 to 0.51 for CF_X-C_8-HT. In addition, I_{2D}/I_G ratio was 0.51 for CF_X-C_8, increasing to 0.73 for CF_X-C_8-HT. These changes are directly attributed to the removal of sp^3 bonded fluorine atoms which disrupt the sp^2 structure of graphitic carbon [34,80]. Overall, these results suggest that the secondary thermal treatment of these fluorinated carbons successfully removes C–F bonds, whilst creating a highly graphitic carbon with unusually large d-spacing.

Finally, attempts were made to measure the WCA of the C_X-CF_8-HT sample after secondary heat treatment. However, for this sample droplet formation was not possible, and the liquid rapidly wetted the surface. As such, the sample is confirmed to be hydrophilic after thermal annealing. Since the microstructure is similar after secondary heat treatment, this confirms that the hydrophobic nature of the synthesised carbons can also be controlled via thermal annealing. This presents a second method of tailoring the hydrophobicity of these fluorinated carbons.

4. Conclusion

In this paper a simple method to synthesize hydrophobic fluorinated carbons with controllable fluorine content was described. Four different fluorotelomer alcohols with different chain length were used as precursors and these were reacted with sodium metal at 150 °C. The reaction was exothermic and the temperature inside the reaction vessel reached 345 °C in one case. The resulting fluorinated carbon nanoparticles had a non-porous microstructure and low surface area, with covalently bonded fluorine content ranging from 5.5 to 9.9 at. % near the surface, depending on the chain length of the fluorotelomer alcohol precursor. It was proposed that the samples are made up of an

amorphous carbon core, with a combination of fluorinated carbon and graphitised carbon near the surface. The highly crystalline graphitic components were present, despite the low reaction temperature, attributed to the catalytic effect of HF generated during the reaction. The carbons were all found to be highly hydrophobic, and the apparent water contact angle was dependant on the fluorine content. Furthermore, secondary thermal treatment was used to effectively remove fluorine atoms from the samples, providing a second method of tailoring the fluorine content and water contact angle.

CRediT authorship contribution statement

Enes Muhammet Can: Methodology, Investigation, Conceptualization, Visualization, Data curation, Writing- original draft. **Masamichi Nishihara:** Resources, Validation, Formal analysis, Investigation. **Junko Matsuda:** Investigation. **Kazunari Sasaki:** Data curation, Funding acquisition. **Stephen Matthew Lyth:** Project administration, Supervision, Validation, Resources, Data curation, Writing-review & editing.

Declaration of Competing Interest

The authors declare that they have no known competing financial interests or personal relationships that could have appeared to influence the work reported in this paper.

Data availability

No data was used for the research described in the article.

Acknowledgments

Part of this study was supported by NEDO (Contract No. JPNP20003). Enes Muhammet Can acknowledges the Ph.D. scholarship funding provided by the Ministry of Education of Türkiye.

Appendix A. Supplementary material

Supplementary data to this article can be found online at https://doi.org/10.1016/j.apsusc.2023.157136.

References

[1] O.R. Brown, Graphite Fluorides (1989), https://doi.org/10.1016/0013-4686(89)87102-6.
[2] R.L. Fusaro, Mechanisms of graphite fluoride [(CFx)n] lubrication, Wear 53 (1979) 303–323, https://doi.org/10.1016/0043-1648(79)90084-X.
[3] T. Nakajima, V. Gupta, Y. Ohzawa, M. Koh, R.N. Singh, A. Tressaud, E. Durand, Electrochemical behavior of plasma-fluorinated graphite for lithium ion batteries, J Power Sources 104 (2002) 108–114, https://doi.org/10.1016/S0378-7753(01)00895-3.
[4] J. Li, K. Naga, Y. Ohzawa, T. Nakajima, H. Iwata, Surface fluorination and electrochemical behavior of petroleum cokes graphitized at medium and high temperatures for secondary lithium battery, J. Fluor. Chem. 126 (2005) 1028–1035, https://doi.org/10.1016/j.jfluchem.2005.03.016.
[5] K. Guérin, M. Dubois, A. Houdayer, A. Hamwi, Applicative performances of fluorinated carbons through fluorination routes: a review, J. Fluor. Chem. 134 (2012) 11–17, https://doi.org/10.1016/j.jfluchem.2011.06.013.
[6] W. Kang, S. Li, Preparation of fluorinated graphene to study its gas sensitivity, RSC Adv. 8 (2018) 23459–23467, https://doi.org/10.1039/C8RA03451F.
[7] E.M. Can, A. Mufundirwa, P. Wang, S. Iwasaki, T. Kitahara, H. Nakajima, M. Nishihara, K. Sasaki, S.M. Lyth, Superhydrophobic fluorinated carbon powders for improved water management in hydrogen fuel cells, J. Power Sources 548 (2022), 232098, https://doi.org/10.1016/j.jpowsour.2022.232098.
[8] J. Guo, J. Zhang, H. Zhao, Y. Fang, K. Ming, H. Huang, J. Chen, X. Wang, Fluorine-doped graphene with an outstanding electrocatalytic performance for efficient oxygen reduction reaction in alkaline solution, R. Soc. Open Sci. 5 (2018), https://doi.org/10.1098/rsos.180925.
[9] S.M. Lyth, W. Ma, J. Liu, T. Daio, K. Sasaki, A. Takahara, B. Ameduri, Solvothermal synthesis of superhydrophobic hollow carbon nanoparticles from a fluorinated alcohol, Nanoscale 7 (2015) 16087–16093, https://doi.org/10.1039/c5nr03484a.
[10] G. Nansé, E. Papirer, P. Fioux, F. Moguet, A. Tressaud, Fluorination of carbon blacks: an X-ray photoelectron spectroscopy study: I. A literature review of XPS studies of fluorinated carbons. XPS investigation of some reference compounds, Carbon N Y. 35 (1997) 175–194, https://doi.org/10.1016/S0008-6223(96)00095-4.
[11] J. Parmentier, S. Schlienger, M. Dubois, E. Disa, F. Masin, T.A. Centeno, Structural/textural properties and water reactivity of fluorinated activated carbons, Carbon N Y. 50 (2012) 5135–5147, https://doi.org/10.1016/j.carbon.2012.06.054.
[12] S.J. Park, M.K. Seo, Y.S. Lee, Surface characteristics of fluorine-modified PAN-based carbon fibers, Carbon N Y. 41 (2003) 723–730, https://doi.org/10.1016/S0008-6223(02)00384-6.
[13] C. Te Hsieh, W.Y. Chen, F.L. Wu, Fabrication and superhydrophobicity of fluorinated carbon fabrics with micro/nanoscaled two-tier roughness, Carbon N Y. 46 (2008) 1218–1224, https://doi.org/10.1016/j.carbon.2008.04.026.
[14] N.O.V. Plank, L. Jiang, R. Cheung, Fluorination of carbon nanotubes in CF4 plasma, Appl. Phys. Lett. 83 (2003) 2426–2428, https://doi.org/10.1063/1.1611621.
[15] C.B. Huffman, E.T. Mickelson, Fluorination of single-wall carbon nanotubes, Chem. Phys. Lett. 296 (1998) 188–194. 10.1016/S0008-6223(97)00013-4.
[16] B. Shen, J. Chen, X. Yan, Q. Xue, Synthesis of fluorine-doped multi-layered graphene sheets by arc-discharge, RSC Adv. 2 (2012) 6761–6764, https://doi.org/10.1039/c2ra20593a.
[17] Y. Ahmad, N. Batisse, X. Chen, M. Dubois, Preparation and applications of fluorinated graphenes, C (Basel) 7 (2021) 20, https://doi.org/10.3390/c7010020.
[18] X. Wang, Y. Dai, J. Gao, J. Huang, B. Li, C. Fan, J. Yang, X. Liu, High-yield production of highly fluorinated graphene by direct heating fluorination of graphene-oxide, ACS Appl. Mater. Interfaces 5 (2013) 8294–8299, https://doi.org/10.1021/am402958p.
[19] W. Zhang, P. Bonnet, M. Dubois, C.P. Ewels, K. Guérin, E. Petit, J.Y. Mevellec, L. Vidal, D.A. Ivanov, A. Hamwi, Comparative study of SWCNT fluorination by atomic and molecular fluorine, Chem. Mater. 24 (2012) 1744–1751, https://doi.org/10.1021/cm203415e.
[20] E. Rangasamy, J. Li, G. Sahu, N. Dudney, C. Liang, Pushing the theoretical limit of Li-CF, J. Am. (2014).
[21] R. Stine, W.K. Lee, K.E. Whitener, J.T. Robinson, P.E. Sheehan, Chemical stability of graphene fluoride produced by exposure to XeF 2, Nano Lett. 13 (2013) 4311–4316, https://doi.org/10.1021/nl4021039.
[22] T. Lim, S. Ju, Control of graphene surface wettability by using CF 4 plasma, Surf. Coat. Technol. 328 (2017) 89–93, https://doi.org/10.1016/j.surfcoat.2017.08.044.
[23] G. Lota, J. Tyczkowski, R. Kapica, K. Lota, E. Frackowiak, Carbon materials modified by plasma treatment as electrodes for supercapacitors, J. Power Sources 195 (2010) 7535–7539, https://doi.org/10.1016/j.jpowsour.2009.12.019.
[24] L. Valentini, Formation of unzipped carbon nanotubes by CF4 plasma treatment, Diam. Relat. Mater. 20 (2011) 445–448, https://doi.org/10.1016/j.diamond.2011.01.038.
[25] D. Tashima, K. Kurosawatsu, M. Uota, T. Karashima, Y.M. Sung, M. Otsubo, C. Honda, Plasma surface treatment of carbonaceous materials for application in electric double layer capacitors, Japan. J. Appl. Phys. 1: Regular Pap. Short Notes Rev. Pap. 45 (2006) 8521–8524, https://doi.org/10.1143/JJAP.45.8521.
[26] A. Felten, A. Eckmann, J.J. Pireaux, R. Krupke, C. Casiraghi, Controlled modification of mono- and bilayer graphene in O2, H2 and CF4 plasmas, Nanotechnology 24 (2013), https://doi.org/10.1088/0957-4484/24/35/355705.
[27] G. Liu, Fluorination of alkenes and alkynes for preparing alkyl fluorides, in: Fluorination, Springer Singapore, 2018, pp. 1–35. 10.1007/978-981-10-1855-8_5-1.
[28] M. Rueda-Becerril, C. Chatalova Sazepin, J.C.T. Leung, T. Okbinoglu, P. Kennepohl, J.F. Paquin, G.M. Sammis, Fluorine transfer to alkyl radicals, J. Am. Chem. Soc. 134 (2012) 4026–4029, https://doi.org/10.1021/ja211679v.
[29] Y.S. Lee, Syntheses and properties of fluorinated carbon materials, J. Fluor. Chem. 128 (2007) 392–403, https://doi.org/10.1016/j.jfluchem.2006.11.014.
[30] O.V. Boltalina, T. Nakajima, New Fluorinated Carbons: Fundamentals and Applications Progress in Fluorine Science Series, 2016.
[31] S. Ha, C. Lim, Y.S. Lee, Fluorination methods and the properties of fluorinated carbon materials for use as lithium primary battery cathode materials, J. Ind. Eng. Chem. 111 (2022) 1–17, https://doi.org/10.1016/j.jiec.2022.03.044.
[32] Y. Ahmad, E. Disa, K. Guérin, M. Dubois, E. Petit, A. Hamwi, P. Thomas, J. L. Mansot, Structure control at the nanoscale in fluorinated graphitized carbon blacks through the fluorination route, J. Fluor. Chem. 168 (2014) 163–172, https://doi.org/10.1016/j.jfluchem.2014.09.021.
[33] H. Touhara, Property control of carbon materials by fluorination, Carbon Alloys: Novel Concepts Dev. Carbon Sci. Technol. 38 (2003) 485–498, https://doi.org/10.1016/B978-008044163-4/50030-9.
[34] S.D. Costa, J.E. Weis, O. Frank, Z. Bastl, M. Kalbac, Thermal treatment of fluorinated graphene: an in situ Raman spectroscopy study, Carbon N. Y. 84 (2015) 347–354, https://doi.org/10.1016/j.carbon.2014.12.029.
[35] Fluorographene: A Two-Dimensional Counterpart of Teflon - Nair - 2010 - Small - Wiley Online Library, (n.d.).
[36] W. Zhang, L. Spinelle, M. Dubois, K. Guérin, H. Kharbache, F. Masin, A. P. Kharitonov, A. Hamwi, J. Brunet, C. Varenne, A. Pauly, P. Thomas, D. Himmel, J.L. Mansot, New synthesis methods for fluorinated carbon nanofibres and applications, J. Fluor. Chem. 131 (2010) 676–683, https://doi.org/10.1016/j.jfluchem.2010.02.007.
[37] S.M. Lyth, H. Shao, J. Liu, K. Sasaki, E. Akiba, Hydrogen adsorption on graphene foam synthesized by combustion of sodium ethoxide, Int. J. Hydrogen Energy 39 (2014) 376–380, https://doi.org/10.1016/j.ijhydene.2013.10.044.
[38] M.I.M. Kusdhany, Z. Ma, A. Mufundirwa, H.W. Li, K. Sasaki, A. Hayashi, S.M. Lyth, Hydrogen and carbon dioxide uptake on scalable and inexpensive microporous

carbon foams, Micropor. Mesopor. Mater. 343 (2022), 112141, https://doi.org/10.1016/j.micromeso.2022.112141.
[39] M.I. Maulana Kusdhany, S.M. Lyth, New insights into hydrogen uptake on porous carbon materials via explainable machine learning, Carbon N. Y. 179 (2021) 190–201, https://doi.org/10.1016/j.carbon.2021.04.036.
[40] J. Liu, D. Takeshi, K. Sasaki, S.M. Lyth, Defective graphene foam: a platinum catalyst support for PEMFCs, J. Electrochem. Soc. 161 (2014) F838–F844, https://doi.org/10.1149/2.0231409jes.
[41] S. Ma, J. Liu, K. Sasaki, S.M. Lyth, P.J.A. Kenis, Carbon foam decorated with silver nanoparticles for electrochemical CO2 conversion, Energy Technology 5 (2017) 861–863, https://doi.org/10.1002/ente.201600576.
[42] J. Liu, B.V. Cunning, T. Daio, A. Mufundirwa, K. Sasaki, S.M. Lyth, Nitrogen-doped carbon foam as a highly durable metal-free electrocatalyst for the oxygen reduction reaction in alkaline solution, Electrochim. Acta 220 (2016) 554–561, https://doi.org/10.1016/j.electacta.2016.10.090.
[43] S.M. Lyth, Y. Nabae, S. Moriya, S. Kuroki, M.A. Kakimoto, J.I. Ozaki, S. Miyata, Carbon nitride as a nonprecious catalyst for electrochemical oxygen reduction, J. Phys. Chem. C 113 (2009) 20148–20151, https://doi.org/10.1021/jp907928j.
[44] S.M. Lyth, Y. Nabae, N.M. Islam, T. Hayakawa, S. Kuroki, M.A. Kakimoto, S. Miyata, Solvothermal synthesis of nitrogen-containing graphene for electrochemical oxygen reduction in acid media, E-J. Surface Sci. Nanotechnol. 10 (2012) 29–32, https://doi.org/10.1380/ejssnt.2012.29.
[45] H.R.M. Jhong, C.E. Tornow, B. Smid, A.A. Gewirth, S.M. Lyth, P.J.A. Kenis, A nitrogen-doped carbon catalyst for electrochemical CO2 conversion to CO with high selectivity and current density, ChemSusChem 10 (2017) 1094–1099, https://doi.org/10.1002/cssc.201600843.
[46] R.C. Buck, J. Franklin, U. Berger, J.M. Conder, I.T. Cousins, P. De Voogt, A. A. Jensen, K. Kannan, S.A. Mabury, S.P.J. van Leeuwen, Perfluoroalkyl and polyfluoroalkyl substances in the environment: terminology, classification, and origins, Integr. Environ. Assess. Manag. 7 (2011) 513–541, https://doi.org/10.1002/ieam.258.
[47] M. Thommes, K. Kaneko, A.V. Neimark, J.P. Olivier, F. Rodriguez-Reinoso, J. Rouquerol, K.S.W. Sing, Physisorption of gases, with special reference to the evaluation of surface area and pore size distribution (IUPAC Technical Report), Pure Appl. Chem. 87 (2015) 1051–1069, https://doi.org/10.1515/pac-2014-1117.
[48] A. Mufundirwa, G.F. Harrington, M.S. Ismail, B. Šmid, B. v. Cunning, Y. Shundo, M. Pourkashanian, K. Sasaki, A. Hayashi, S.M. Lyth, Gram-scale synthesis of alkoxide-derived nitrogen-doped carbon foam as a support for Fe-N-C electrocatalysts, Nanotechnology 31 (2020) 10.1088/1361-6528/ab76ed.
[49] J.T. Robinson, J.S. Burgess, C.E. Junkermeier, S.C. Badescu, T.L. Reinecke, F. K. Perkins, M.K. Zalalutdniov, J.W. Baldwin, J.C. Culbertson, P.E. Sheehan, E. S. Snow, Properties of fluorinated graphene films, Nano Lett. 10 (2010) 3001–3005, https://doi.org/10.1021/nl101437p.
[50] A. Tressaud, F. Moguet, S. Flandrois, M. Chambon, C. Guimon, G. Nanse, E. Papirer, V. Gupta, O.P. Bahl, On the nature of C-F bonds in various fluorinated carbon materials: XPS and TEM investigations, J. Phys. Chem. Solids 57 (1996) 745–751, https://doi.org/10.1016/0022-3697(96)00343-5.
[51] D. Wang, J. Peng, Y. Huang, L. Sun, M. Liu, H. Li, M. Chao, P. Gong, Z. Liu, J. You, Rational construction of fluorescence turn-off fluorinated carbon fiber/Ag composites and their anticancer and antibacterial activities, ACS Appl. Bio Mater. 4 (2021) 1749–1759, https://doi.org/10.1021/acsabm.0c01503.
[52] P. Gong, S. Ji, J. Wang, D. Dai, F. Wang, M. Tian, L. Zhang, F. Guo, Z. Liu, Fluorescence-switchable ultrasmall fluorinated graphene oxide with high near-infrared absorption for controlled and targeted drug delivery, Chem. Eng. J. 348 (2018) 438–446, https://doi.org/10.1016/j.cej.2018.04.193.
[53] D. Wang, Y. Zhang, M. Zhai, Y. Huang, H. Li, X. Liu, P. Gong, Z. Liu, J. You, Fluorescence turn-off magnetic fluorinated graphene composite with high NIR absorption for targeted drug delivery, ChemNanoMat 7 (2021) 71–77, https://doi.org/10.1002/cnma.202000539.
[54] C. Li, P. Gong, M. Chao, J. Li, L. Yang, Y. Huang, D. Wang, J. Liu, Z. Liu, A biomimetic lubricating nanosystem with responsive drug release for osteoarthritis synergistic therapy, Adv. Healthc. Mater. (2023) 2203245, https://doi.org/10.1002/adhm.202203245.
[55] Y. Huang, P. Gong, M. Liu, J. Peng, R. Zhang, C. Qi, Y. Hou, M. Liu, D. Wang, Z. Liu, Near-infrared light enhanced starvation therapy to effectively promote cell apoptosis and inhibit migration, Mater. Adv. 2 (2021) 3981–3992, https://doi.org/10.1039/d1ma00148e.
[56] J. Si, R. Ma, Y. Wu, Y. Dong, K. Yao, Microstructure and magnetic properties of novel powder cores composed of iron-based amorphous alloy and PTFE, J. Mater. Sci. 57 (2022) 8154–8166, https://doi.org/10.1007/s10853-022-07199-4.
[57] W. Zhao, C. Song, B. Zheng, J. Liu, T. Viswanathan, Thermal recovery behavior of fluorinated single-walled carbon nanotubes, J. Phys. Chem. B 106 (2002) 293–296, https://doi.org/10.1021/jp0133135.
[58] R.R. Nair, W. Ren, R. Jalil, I. Riaz, V.G. Kravets, L. Britnell, P. Blake, F. Schedin, A. S. Mayorov, S. Yuan, M.I. Katsnelson, H.-M. Cheng, W. Strupinski, L.G. Bulusheva, A.V. Okotrub, I.V. Grigorieva, A.N. Grigorenko, K.S. Novoselov, A.K. Geim, Fluorographene: a two-dimensional counterpart of teflon, Small 6 (2010) 2877–2884, https://doi.org/10.1002/smll.201001555.
[59] Y. Sato, H. Watano, R. Hagiwara, Y. Ito, Reaction of layered carbon fluorides CxF (x = 2.5-3.6) and hydrogen, Carbon N. Y. 44 (2006) 664–670, https://doi.org/10.1016/j.carbon.2005.09.029.
[60] B.H.F. Mcmurdie, M.C. Morris, E.H. Evans, B. Paretzkin, W. Wong-ng, Y. Zhang, C. R. Hubbard, Standard X-ray diffraction powder patterns from the JCPDS research associateship — international centre for diffraction data ammonium hydrogen phosphate, NH4H2PO4 barium magnesium germanium oxide, Powder Diffr. 1 (1986) 334–345.
[61] A.C. Ferrari, Raman spectroscopy of graphene and graphite: disorder, electron-phonon coupling, doping and nonadiabatic effects, Solid State Commun. 143 (2007) 47–57, https://doi.org/10.1016/j.ssc.2007.03.052.
[62] A.C. Ferrari, J.C. Meyer, V. Scardaci, C. Casiraghi, M. Lazzeri, F. Mauri, S. Piscanec, D. Jiang, K.S. Novoselov, S. Roth, A.K. Geim, Raman spectrum of graphene and graphene layers, Phys. Rev. Lett. 97 (2006) 1–4, https://doi.org/10.1103/PhysRevLett.97.187401.
[63] J. Ek Weis, S.D. Costa, O. Frank, Z. Bastl, M. Kalbac, Fluorination of isotopically labeled turbostratic and bernal stacked bilayer graphene, Chem. – Eur. J. 21 (2015) 1081–1087, https://doi.org/10.1002/chem.201404813.
[64] A. Sadezky, H. Muckenhuber, H. Grothe, R. Niessner, U. Pöschl, Raman microspectroscopy of soot and related carbonaceous materials: spectral analysis and structural information, Carbon N. Y. 43 (2005) 1731–1742, https://doi.org/10.1016/j.carbon.2005.02.018.
[65] J.J. Kipling, J.N. Sherwood, P.V. Shooter, N.R. Thompson, Factors influencing the graphitization of polymer carbons, Carbon N. Y. 1 (1964), https://doi.org/10.1016/0008-6223(64)90285-4.
[66] S.M. Lyth, S.R.P. Silva, Electron field emission from water-based carbon nanotube inks, ECS J. Solid State Sci. Technol. 4 (2015) P3034–P3043, https://doi.org/10.1149/2.0051504jss.
[67] M.B. Smith, Chapter 16 - Carbon-Carbon Bond-Forming Reactions: Carbocation and Oxocarbenium Ion Intermediates, 2017.
[68] N. Hansen, T. Brüggemann, A.T. Bell, F.J. Keil, Theoretical investigation of benzene alkylation with ethene over H-ZSM-5, J. Phys. Chem. C 112 (2008) 15402–15411, https://doi.org/10.1021/jp8036022.
[69] Y. Liu, L. Xu, B. Xu, Z. Li, L. Jia, W. Guo, Toluene alkylation with 1-octene over supported heteropoly acids on MCM-41 catalysts, J. Mol. Catal. A Chem. 297 (2009) 86–92, https://doi.org/10.1016/j.molcata.2008.09.007.
[70] V.H. Dalvi, P.J. Rossky, Molecular origins of fluorocarbon hydrophobicity, Proc. Natl. Acad. Sci. U S A 107 (2010) 13603–13607, https://doi.org/10.1073/pnas.0915169107.
[71] V. Mulone, K. Karan, Analysis of capillary flow driven model for water transport in PEFC cathode catalyst layer: consideration of mixed wettability and pore size distribution, Int. J. Hydrogen Energy 38 (2013) 558–569, https://doi.org/10.1016/j.ijhydene.2012.07.107.
[72] W. Olbrich, T. Kadyk, U. Sauter, M. Eikerling, Modeling of wetting phenomena in cathode catalyst layers for PEM fuel cells, Electrochim. Acta 431 (2022), 140850, https://doi.org/10.1016/j.electacta.2022.140850.
[73] W. Olbrich, T. Kadyk, U. Sauter, M. Eikerling, Review—wetting phenomena in catalyst layers of PEM fuel cells: novel approaches for modeling and materials research, J. Electrochem. Soc. 169 (2022), 054521, https://doi.org/10.1149/1945-7111/ac6e8b.
[74] E. Disa, M. Dubois, K. Guérin, H. Kharbache, F. Masin, A. Hamwi, The effect of nanostructure on the thermal properties of fluorinated carbon nanofibres, Carbon N. Y. 49 (2011) 4801–4811, https://doi.org/10.1016/j.carbon.2011.06.092.
[75] P.E. Pehrsson, W. Zhao, J.W. Baldwin, C. Song, J. Liu, S. Kooi, B. Zheng, Thermal fluorination and annealing of single-wall carbon nanotubes, J. Phys. Chem. B 107 (2003) 5690–5695, https://doi.org/10.1021/jp027233s.
[76] A. Oberlin, Carbonization and graphitization, Carbon N. Y. 22 (1984) 521–541, https://doi.org/10.1016/0008-6223(84)90086-1.
[77] W. Zhang, M. Dubois, K. Guérin, P. Bonnet, E. Petit, N. Delpuech, D. Albertini, F. Masin, A. Hamwi, Effect of graphitization on fluorination of carbon nanocones and nanodiscs, Carbon N. Y. 47 (2009) 2763–2775, https://doi.org/10.1016/j.carbon.2009.05.035.
[78] A. Tressaud, E. Durand, C. Labrugère, A.P. Kharitonov, L.N. Kharitonova, Modification of surface properties of carbon-based and polymeric materials through fluorination routes: from fundamental research to industrial applications, J. Fluor. Chem. 128 (2007) 378–391, https://doi.org/10.1016/j.jfluchem.2006.12.015.
[79] J.C. Agopian, O. Téraube, K. Charlet, M. Dubois, A review about the fluorination and oxyfluorination of carbon fibres, J. Fluor. Chem. 251 (2021), https://doi.org/10.1016/j.jfluchem.2021.109887.
[80] C. Casiraghi, Doping dependence of the Raman peaks intensity of graphene close to the Dirac point, Phys. Rev. B Condens. Matter Mater. Phys. 80 (2009) 2–4, https://doi.org/10.1103/PhysRevB.80.233407.